

Article

# In One Fell Sweep: Modeling Exchange, Hyperfine and Dipolar Interactions from EPR Spectra of Copper(II) Spin Triangles

Athanasios K. Boudalis <sup>†</sup> 

Strasbourg Institute of Chemistry (UMR 7177, CNRS-Unistra), University of Strasbourg, 4 rue Blaise Pascal, CS 90032, F-67081 Strasbourg, France; bountalis@unistra.fr

<sup>†</sup> Dedicated to Dr. Romain Ruppert on the occasion of his retirement.

**Abstract:** The weak intramolecular magnetic interactions within a series of Cu<sup>II</sup><sub>3</sub> complexes based on the trinucleating 2,4,6-tris(di-2-pyridylamino)-1,3,5-triazine (dipyatriz) ligand were investigated via Electron Paramagnetic Resonance (EPR) spectroscopy. X- and Q-band EPR spectroscopy in powders and frozen solutions were recorded and the Q-band spectra were interpreted by a multispin Hamiltonian model comprising exchange, dipolar and hyperfine interactions. The described methodology is suitable for the elucidation of weak intramolecular interactions which are not amenable to analysis via magnetic susceptibility studies.

**Keywords:** EPR spectroscopy; spin triangles; dipolar interactions; hyperfine interactions; spin Hamiltonian

## 1. Introduction

Spin triangles constitute a “rediscovered” class of metal complexes [1], whose magnetic properties have rendered them interesting as potential magnetoelectric materials [2–6], with a proposed use as electrically controlled and slow-decoherence spin-chirality qubits [7–10].

Our overall ability to design and implement such devices is predicated on our precise understanding of their magnetic structures, down to the finest details. Traditionally, the general strategy implemented to tackle this task is the same as with most other molecular magnetic materials: magnetometric techniques (e.g., SQUID magnetometry) are first used to elucidate the gross magnetic structure governed by isotropic (Heisenberg–Dirac–van Vleck) interactions and eventually antisymmetric (Dzyaloshinskii–Moriya) interactions, both of superexchange origins. Finer terms, such as zero-field splitting (zfs) or anisotropic interactions, are not very reliably assessed via magnetometric techniques, necessitating the use of spectroscopic techniques, the most prominent of which is Electron Paramagnetic Resonance (EPR) spectroscopy.

The use of EPR spectroscopy has its own limitations, e.g., when dealing with non-Kramers systems and very large zfs terms. While these systems are addressable through high-frequency (W-band frequencies and above) or THz EPR, the availability of such experiments can be a limiting factor to their use. Classical EPR, however, i.e., at Q-band frequencies and below, can yield very precise information on weaker terms, such as hyperfine interactions. In addition, low-temperature studies can yield very informative data on the ground states of polynuclear complexes, which then can be used to verify the magnetometry-derived conclusions regarding exchange interactions [11].

The above strategy works very nicely in cases where  $J \gg k_B T$ ,  $A$ , i.e., at the strong exchange limit. When, however, exchange interactions are very weak with respect to the thermal energy and comparable to eventual hyperfine interactions, errors in magnetometric techniques (weighing, diamagnetic corrections) render their use problematic. The large diamagnetic content of biological magnetic systems can give rise to such problems even for strong exchange interactions. In such cases, EPR spectroscopy can often yield useful information. However, a careful construction of the model is then required to include



**Citation:** Boudalis, A.K. In One Fell Sweep: Modeling Exchange, Hyperfine and Dipolar Interactions from EPR Spectra of Copper(II) Spin Triangles. *Magnetochemistry* **2023**, *9*, 217. <https://doi.org/10.3390/magnetochemistry9100217>

Academic Editor: Angeliki Giannoulis

Received: 8 September 2023

Revised: 27 September 2023

Accepted: 29 September 2023

Published: 6 October 2023



**Copyright:** © 2023 by the author. Licensee MDPI, Basel, Switzerland. This article is an open access article distributed under the terms and conditions of the Creative Commons Attribution (CC BY) license (<https://creativecommons.org/licenses/by/4.0/>).

any term that might influence the EPR spectrum. These include not just isotropic interactions, but also the full description of the system symmetry that influences its anisotropic terms. These may include Dzyaloshinskii–Moriya interactions (DMI), dipolar interactions, anisotropic exchange and hyperfine interactions, taking proper care to model the various tensor orientations (e.g.,  $\tilde{\mathbf{g}}$ ,  $\mathbf{A}$ , etc.) and vectors connecting the different spins.

In a previous work, we showed that it is possible to derive very accurate descriptions of the magnetic properties of trinuclear  $\text{Cu}^{\text{II}}$  complexes [12] by properly accounting for the dipolar terms, which induce a zfs in their quartet states. Such studies are not only applicable on single-crystal data, but also to those from randomly oriented samples (powders or frozen solutions). In those previous cases, hyperfine interactions were not considered, either because they were unresolved or because they were very weak, respectively. Moreover, it was considered that their inclusion might render the problem computationally intractable; in the case of  $\text{Cu}^{\text{II}}_3$ , the Hilbert space would reach a dimension of  $(2S + 1)^n \times (2I + 1)^m = 512$  for  $S = 1/2$  ( $\text{Cu}^{\text{II}}$ ),  $I = 3/2$  (for  $^{63/65}\text{Cu}$ ), and for  $n = m = 3$  electron and nuclear spins, further complicated by the need to calculate  $2^3 = 8$  possible isotopologs for the  $^{63/65}\text{Cu}$  nuclei.

The renewed interest in spin triangles as spin-chirality qubits involves the excitation of the “chiral transitions” *between*, not *within*, the low-lying spin doublets. Therefore, engineering the interdoublet energy gap  $\Delta$  becomes a question of interest. For spin triangles with monatomic bridges (e.g.,  $\text{O}^{2-}$ ,  $\text{OH}^-$ ,  $\text{RO}^-$ ), this can be in the order of  $\sim 10^2 \text{ cm}^{-1}$  for  $\text{Cu}^{\text{II}}_3$  triangles,  $\sim 10^1 \text{ cm}^{-1}$  for  $\text{Fe}^{\text{III}}_3$  triangles and  $\sim 10^0 \text{ cm}^{-1}$  for  $\text{Cr}^{\text{III}}$  triangles, i.e., in the THz and FIR regimes. Large trinucleating ligands in place of monatomic ones impose larger interspin separations, allowing us to eventually modulate this energy and lower it within the GHz regime, which is more tractable using EPR instrumentation.

Ligand 2,4,6-tris(di-2-pyridylamino)-1,3,5-triazine (dipyatriz) has in the past been used to construct such molecular architectures. Its attractiveness in copper(II) chemistry lies in the fact that the axial ligands of copper(II) ions can be easily changed by proper the choice of synthetic conditions, namely the relative ratios of  $\text{CuCl}_2 \cdot 2\text{H}_2\text{O}$  and  $\text{CuClO}_4 \cdot 6\text{H}_2\text{O}$  starting materials. Exchanging neutral for anionic ligands can therefore rationally modify the total charge of the molecule. Indeed, previously reported complexes include  $[\text{Cu}_3(\text{dipyatriz})_2\text{Cl}_3](\text{ClO}_4)_3$  (**1**) [13],  $[\text{Cu}_3(\text{dipyatriz})_2(\text{H}_2\text{O})\text{Cl}_2](\text{ClO}_4)_4$  (**2**) [13],  $[\text{Cu}_3(\text{dipyatriz})_2(\text{H}_2\text{O})_3](\text{ClO}_4)_6$  (**3**) [14],  $[\text{Cu}_3(\text{dipyatriz})_2\text{Cl}_3][\text{CuCl}_4]\text{Cl}$  (**4**) [15] and  $[\text{Cu}_3(\text{dipyatriz})_2\text{Cl}_3]\text{Cl}_3$  (**5**) [16], with electric charges of the molecules being rationally modifiable from +3 to +6 without noticeably changing the structure of the metal core (although the +5 complex  $[\text{Cu}_3(\text{dipyatriz})_2(\text{H}_2\text{O})_2\text{Cl}](\text{ClO}_4)_5$  has not yet been reported, its synthesis should, in principle, be feasible through the modification of the molecular ratios of  $\text{CuCl}_2 \cdot 2\text{H}_2\text{O}$  and  $\text{Cu}(\text{ClO}_4)_2 \cdot 6\text{H}_2\text{O}$  used for the new synthesis of complex **2** reported here). This feature constitutes a degree of freedom for the control of solubilities in desired solvents.

This was therefore deemed a suitable system to construct spin triangles characterized by moderate to weak interactions, and use EPR spectroscopy to assess their magnetic structures far more accurately than it is possible with magnetometric techniques.

This work describes the modeling of the spin Hamiltonian parameters of a series of  $\text{Cu}^{\text{II}}_3$  spin triangles of similar structures (Figure 1) using continuous-wave (CW) EPR data at the X- and Q-bands. From a general perspective, these results outline a methodology to fully account for features of EPR spectra arising from exchange and dipolar interactions by accurately describing the spatial arrangement of the tensorial and vectorial terms of the multispin Hamiltonian. Moreover, the specific results provide precise estimates of exchange interactions mediated by an extended organic superexchange pathway. Such precise estimates, quite difficult to come by via magnetometric methods, are valuable for the calibration of theoretical methods attempting to derive such exchange terms from first principles.

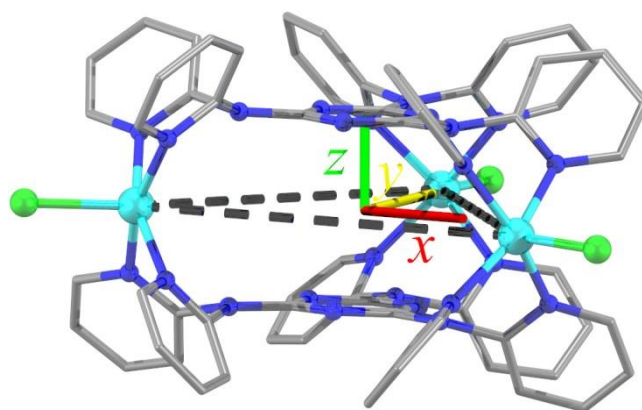


**Figure 1.** POV-Ray plot of the cation of **1** superposed to the molecular reference frame  $R_M$  used in the analysis of its magnetic properties. This is a right-handed reference frame with its origin  $O$  at the center of an idealized equilateral triangle, with  $x \parallel r_{12}$  and  $z$  normal to the triangle plane.

## 2. Results

In the original work [13], no magnetic studies were reported for **1**. For the structurally related complex **4**, SQUID magnetometry yielded antiferromagnetic interactions ( $J = +0.42 \text{ cm}^{-1}$ ) with  $g_{\text{iso}} = 2.04$ ; these results, however, needed to also account for the Curie contribution of the  $[\text{CuCl}_4]^{2-}$  counter-anion, putting the derived values into question due to possible correlations [15]. In a related work, the SQUID magnetometry of **3** also yielded AF interactions, though much weaker, i.e.,  $J = 0.08 \text{ cm}^{-1}$  ( $g_{\text{iso}} = 2.07$ ) [14].

Preliminary EPR studies at the X- and Q-bands in the solid state (Figure 2) revealed largely unresolved spectra for **1** and **2**. These exhibit clear low-field features which disappear upon dissolution. Thus, these might tentatively be attributed to half-field and third-field transitions due to intermolecular dipolar interactions. However, the complexity of simulating EPR spectral features stemming from intermolecular interactions precludes their confident assignment.

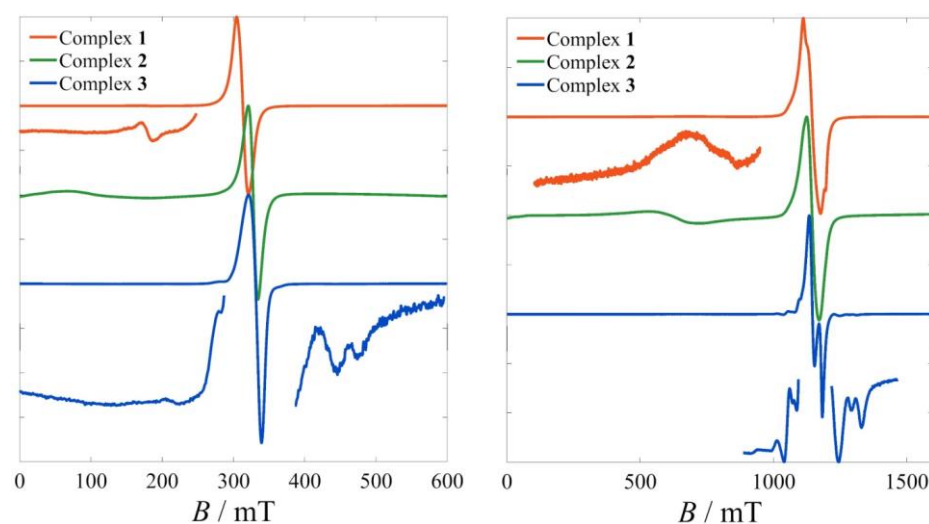


**Figure 2.** Room-temperature powder spectra of **1–3** at the X-band (left) and at the Q-band (right). Only complex **3** shows a partially resolved fine and hyperfine structure.

On the other hand, fine and hyperfine structures are observed in the spectra of **3**, both in the X- and the Q-bands. At the same time, the low-field region (not shown) is completely devoid of any features. The factors influencing EPR spectra in the solid state are more complicated due to the extended intermolecular interactions, but a plausible explanation for the above observations is that the larger intermolecular distances between the hexacations

of **3** must play a role in reducing dipolar broadenings in the solid state. Indeed, the shortest intermolecular Cu...Cu distances are 7.262, 8.829 and 9.686 Å for **1**, **2** and **3**, respectively.

To better understand the magnetic properties of the three complexes, frozen solution studies were also carried out. In the X-band spectra (Figure 3, left), the hyperfine interactions of the  $A_{i||}$  component were partially resolved for **1** and **3**, but not for **2**. The  $g$ -anisotropy was predictably much less resolved for all three. Q-band spectra were then collected at 5 K in the hopes of better resolving the various contributions. Indeed, at that frequency, not only was the  $g$ -anisotropy resolved, but further details emerged (Figure 3, right). First, the perpendicular component of the anisotropy  $A_{i\perp}$  was also resolved, whereas lateral weak absorptions appeared, which were assigned to intermultiplet ( $\Delta S_T = \pm 1$ ) transitions.

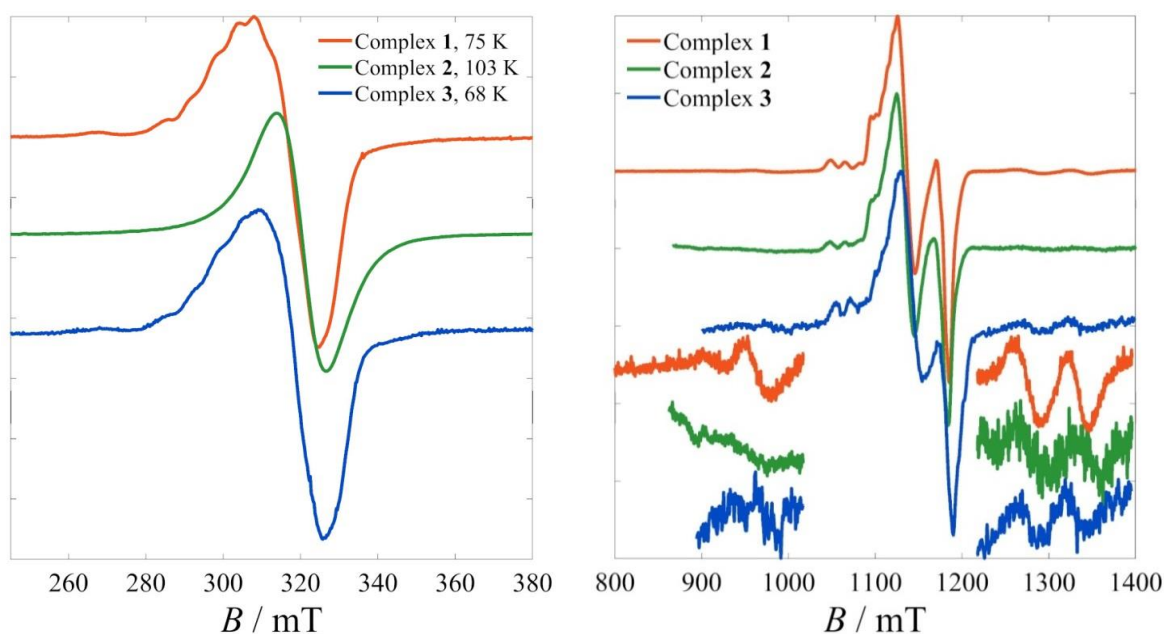


**Figure 3.** Frozen solution EPR spectra of complexes **1–3**. (Left) X-band spectra at the indicated temperatures. (Right) Q-band spectra at 5 K.

These additional features of the Q-band spectra permitted their thorough analysis based on a more elaborate model. Although all three spectra demonstrated the same overall features, the most detailed analysis was carried out on the spectrum of **1**, which exhibited the best S/N ratio.

The selected model comprised an isosceles magnetic symmetry of the isotropic (Heisenberg–Dirac–van Vleck) interactions, dipolar interactions and hyperfine interactions. The full multispin Hamiltonian was:

$$\hat{H} = J(\hat{S}_1 \cdot \hat{S}_2 + \hat{S}_1 \cdot \hat{S}_3) + J'\hat{S}_2 \cdot \hat{S}_3 + \sum_{i,j=1}^3 \hat{S}_i^T \tilde{\mathbf{D}}_{ij}^{dip} \hat{S}_j + \sum_{i=1}^3 \hat{I}_i^T \tilde{\mathbf{A}} \hat{S}_i + \mu_B \mathbf{B}^T \sum_{i=1}^3 \tilde{\mathbf{g}}_i \hat{S}_i$$

For the calculations, the fitted quantities were the average of the  $J$  and  $J'$  values and their difference, defined, respectively, as:  $J_{av} = (2J + J')/3$  and  $\Delta J = J - J'$  (whence it can be derived that  $J = (3J_{av} + \Delta J)/3$  and  $J' = (3J_{av} - 2\Delta J)/3$ ). To avoid overparameterization, the  $g$ - and  $A$ -tensor elements for the three ions were taken as identical, as were the interspin distances. The  $g$ -tensor reference frames were fixed to idealized positions based on the crystal structure, characterized by Euler angles  $\mathbf{E}_{g1} = [90^\circ, 90^\circ, -45^\circ]$ ,  $\mathbf{E}_{g2} = [30^\circ, -90^\circ, 135^\circ]$  and  $\mathbf{E}_{g3} = [-30^\circ, 90^\circ, -45^\circ]$  with respect to the molecular frame ( $\mathbf{E}_{RM} = [0, 0, 0]$ ). The  $A$ -tensors were initialized collinear to their respective  $g$ -tensors ( $\mathbf{E}_{Ai(0)} = \mathbf{E}_{gi}$ ) and were allowed to vary slightly around that position during the fitting process. To avoid

overparameterization, this variation,  $\Delta_A$ , was common for all three hyperfine tensors ( $\mathbf{E}_{Ai} = \mathbf{E}_{Ai(0)} + \Delta_A$ ).

Preliminary fits were carried out with a model assuming two  $^{63}\text{Cu}$  nuclei and one  $^{65}\text{Cu}$  nucleus, which is very close to the natural abundances of the two nuclei (i.e., 69.17% and 30.83%, respectively). Simulations revealed that these were largely superimposable with the spectrum calculated, assuming natural abundances on each site (Figure S1). Since, however, the simulation time rose by a factor of 8 in the latter case due to the calculation of the  $2^3$  possible isotopologs, this calculation was reserved for only the final fits and statistical analyses of the fitted variables (reported below).

The best-fit parameters to this model, along with their 95% confidence intervals, are thus determined to be:  $g_{i||} = 2.25707 \pm 0.00036$ ,  $g_{i\perp} = 2.05853 \pm 0.00021$ ,  $\sigma_G = 2.31 \pm 0.80 \text{ mT}_{\text{pp}}$ ,  $\sigma_L = 2.85 \pm 0.22 \text{ mT}_{\text{pp}}$ ,  $r_{ij} = 8.22 \pm 0.11 \text{ \AA}$ ,  $J_{av} = 0.11217 \pm 0.00050 \text{ cm}^{-1}$ ,  $\Delta J = 0.0114 \pm 0.0018 \text{ cm}^{-1}$ ,  $A_{i||} = 502.94 \pm 8.42 \text{ MHz}$ ,  $A_{i\perp} = 52.0 \pm 13.2 \text{ MHz}$ ,  $\Delta_A = [-6.4 \pm 2.5^\circ, 3.4 \pm 7.4^\circ, 28.8486 \pm 0.0005^\circ]$ . The fit is shown in Figure 4, along with the resonances calculated in the *z*- and *x*-molecular orientations of the magnetic field. The fitted tensor elements are shown in Figure 5.

The fitted transitions involve several intermultiplet ones, whose assignment is facilitated by the consideration of the low-field part of the Zeeman diagram (Figure S2). Briefly, in spin triangles, the spin–spin couplings create magnetic levels whose description can be based on the intermediate spin quantum number  $S_{23}$  (where  $\hat{S}_{23} = \hat{S}_2 + \hat{S}_3$ ), the total spin quantum number  $S$  (where  $\hat{S} = \hat{S}_1 + \hat{S}_{23}$ ) and the quantum number  $M_S$  of the projection of the total spin ( $= +S, +S - 1, \dots, -S$ ). In that scheme,  $S_{23}$  allows us to distinguish between the two spin doublets (e.g., for  $S_i = 1/2$  systems,  $S_{23} = 0$  or  $1$ ). However, in the present case, the two doublets are too closely packed and the resonances too numerous for a clear labeling of the states to be possible with the  $|S_{23}, S, M_S\rangle$  scheme. Instead, the simplified scheme  $|S, M_S\rangle$  is used in Figure 4.

Unsurprisingly, the confidence intervals indicate that the *g*-tensor elements are very well determined. Moreover, we also derive quite small confidence intervals for the average *J* value, whose magnitude closely tracks the positions of the lateral absorptions. The calculated distance is remarkably close to the crystallographically determined distance average of 8.29 Å (from 8.28, 8.46 and 8.12 Å distances), thus validating the hypothesis of the point dipole model. The values of the hyperfine interactions are also quite well determined and yield reasonable values.

One remark concerns the Euler angles of the local hyperfine tensors. The first two rotation angles which, respectively, define the angular deviations from the triangle disector and the triangle plane are predictably small and ill-defined. However, we derive a remarkably narrow confidence interval for the third angle, which defines rotations around the local *z*-axes. This is interpreted more as an artifact of the covariance matrix calculation rather than as a highly certain determination of that angle. While the fits did coherently converge to a significant rotation around the local *z*-axes, and while these are considered as bearing true physical meaning, the narrowness of the associated confidence interval is not considered to be quantitatively reliable.

A feature that was consistently difficult to reproduce was the line width of the lateral absorptions, with the calculated spectra always yielding much sharper line shapes. The inclusion of antisymmetric (Dzyaloshinskii–Moriya) interactions did not improve the agreement with the experiments. A tentative interpretation is that this line shape is associated with distributions of the exchange terms. Indeed, given the relative flexibility of the molecular scaffold, it is plausible to assume the presence of several slightly different conformations of the molecules in solution. These should be associated with slightly distributed  $J_{av}$  and  $\Delta J$  values, which should contribute to this line broadening. A detailed analysis of magnetic exchange parameter distributions would require the calculation of a series of EPR spectra, and would therefore be prohibitively time consuming due to the large Hilbert space of this problem.

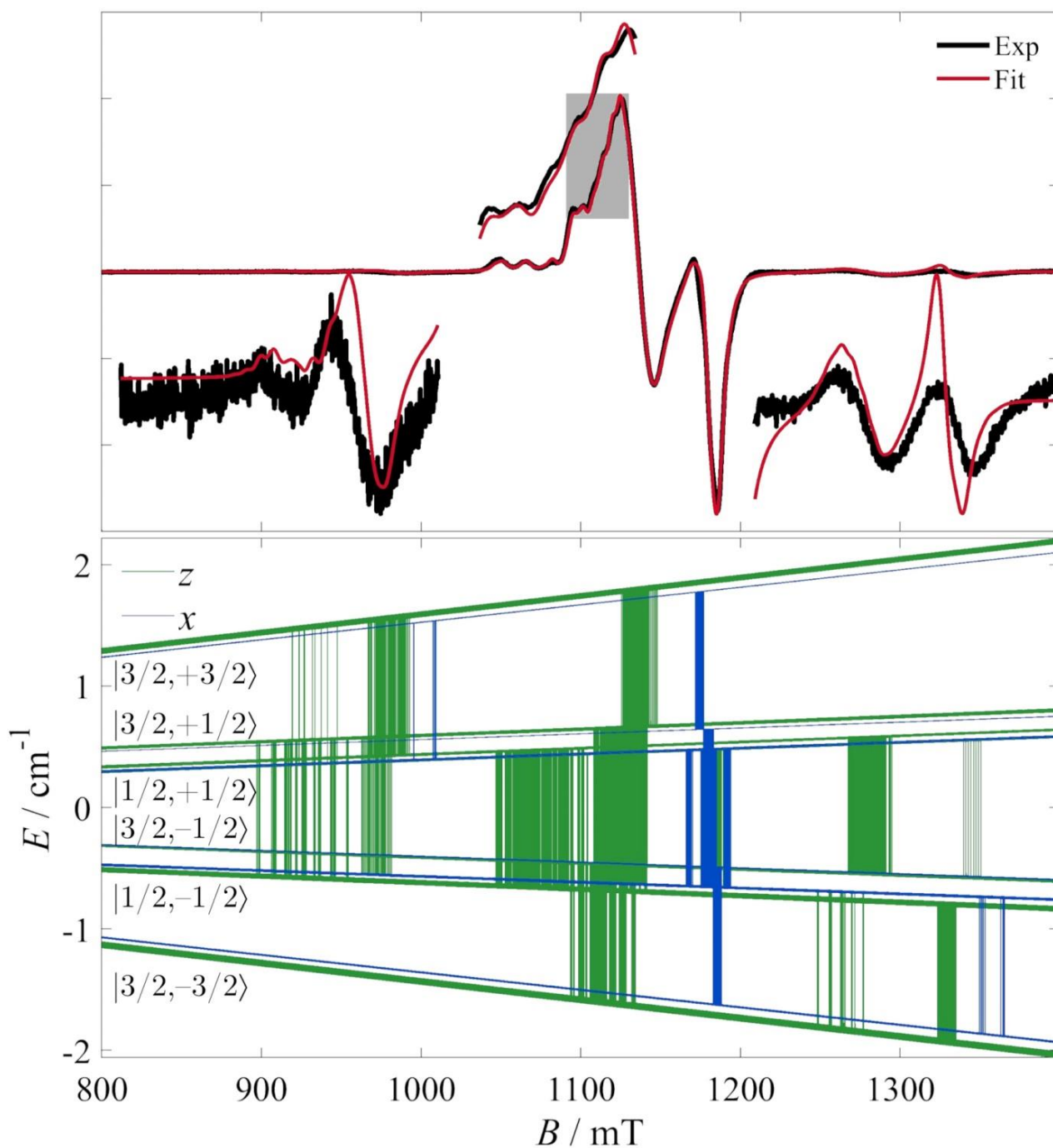


**Figure 4.** (Top) CW EPR spectrum of a frozen solution (5 K) at the Q-band (black lines) and best fit to the model described in the text. The bottom insets are in scale with respect to the  $x$ -axis and expanded only along the  $y$ -axis. The top inset is an expansion of the area around the  $g \sim 2.2$  region indicated by the gray rectangle. (Bottom) Zeeman diagrams and resonances at the  $z$  (green) and  $x$  (blue) orientations in the molecular reference frame. The Zeeman diagram was calculated for an isotopologue with three  $^{63}\text{Cu}$  nuclei and assignments were facilitated by the low-field part of the diagram (Figure S2). The low- and high-field signals correspond to intermultiplet  $\Delta M_S = 1$  transitions. Low-field signals are assigned to  $|S, M_S\rangle = |1/2, -1/2\rangle \rightarrow |3/2, +1/2\rangle$  and  $|1/2, +1/2\rangle \rightarrow |3/2, +3/2\rangle$  transitions, while high-field signals to  $|3/2, -3/2\rangle \rightarrow |1/2, -1/2\rangle$  and  $|3/2, -1/2\rangle \rightarrow |1/2, +1/2\rangle$  transitions.

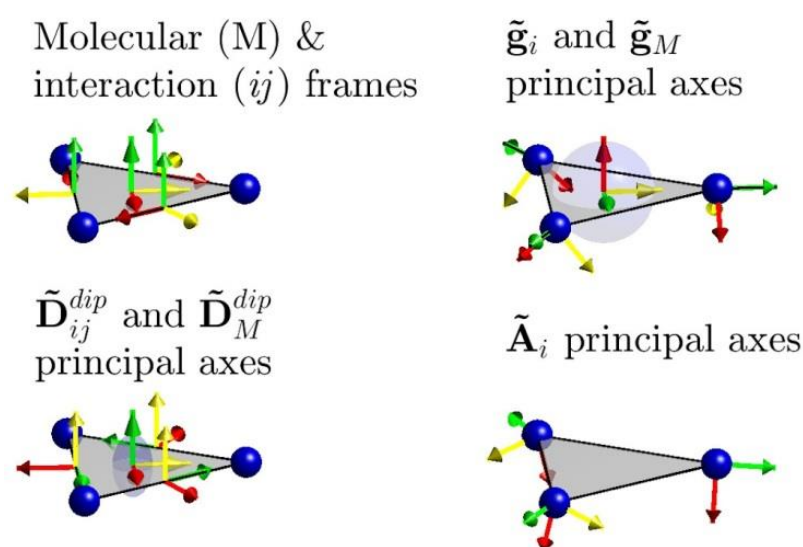


**Figure 5.** Molecular and local reference frames for interactions and tensors used in the spin Hamiltonian. The blue transparent ellipsoids indicate the anisotropy of the  $\mathbf{g}$  and total anisotropy tensors. The latter is derived purely from dipolar interactions.

To validate the model used and to justify the number of terms employed, the effect of each of these terms was demonstrated by simulations shown in Figure 6. The most salient observation is the remarkable effect of the exchange terms on the spectral appearance, both in the central and on the lateral absorptions. Simulations considering only the dipolar contributions or a simple mononuclear paramagnetic species were far from the observed spectrum.

Moreover, it was shown that the dipolar term is also necessary to reproduce the finer details of the central absorption; indeed, neglecting the dipolar terms leads to simulations of visibly lower quality, presumably from the absence of the dipolar-induced zfs in the quartet state.

The least conspicuous effect is that of the  $\Delta J$  term (Heisenberg asymmetry), also reflected on the relatively larger confidence intervals of its fitted value. Indeed, the inclusion of this term mainly affects the appearance of the lateral absorptions, particularly the low-field ones. Although small, however, the role of this term is not insignificant and indicates the power of EPR spectroscopy to detect small differences of already weak exchange terms; indeed, the fitted value of  $0.0114 \text{ cm}^{-1}$  or  $343 \text{ MHz}$  is of the order of magnitude of the hyperfine terms.

The absolute values of the principal tensor elements of the pairwise dipolar interactions at those distances were 228, 104 and  $99 \text{ MHz}$ , yielding a total zfs with  $D_{\text{dip}} = 74 \text{ MHz}$  ( $0.0025 \text{ cm}^{-1}$ ) when the local reference frames are taken into account.

Given the relatively good quality of the Q-band spectrum of **2**, fits were attempted based on the model used for **1** and by using that best-fit solution as a point of departure. However, given the relatively poorer spectral quality, a simplification was made by considering collinear  $\tilde{\mathbf{g}}_i$  and  $\tilde{\mathbf{A}}_i$  local tensors. The best-fit parameters to this model, along with their 95% confidence intervals, are:  $g_{i\parallel} = 2.25488 \pm 0.00061$ ,  $g_{i\perp} = 2.06111 \pm 0.00025$ ,  $\sigma_G = 3.3 \pm 1.0 \text{ mT}_{\text{pp}}$ ,  $\sigma_L = 2.41 \pm 0.50 \text{ mT}_{\text{pp}}$ ,  $r_{ij} = 8.35 \pm 0.15 \text{ \AA}$ ,  $J_{av} = 0.11628 \pm 0.00073 \text{ cm}^{-1}$ ,  $\Delta J = 0.0150 \pm 0.0019 \text{ cm}^{-1}$ ,  $A_{i\parallel} = 543 \pm 14 \text{ MHz}$ ,  $A_{i\perp} = 69.6 \pm 6.4 \text{ MHz}$ .  $\Delta_A$  was fixed to  $[0, 0, 0]$ . The respective calculated spectrum is shown in Figure 7a.

Finally, similar fits were attempted for the powder room-temperature spectra of **3** (Figure 7b), whose fine structure made such fits feasible. It is suggested that the observation of this fine structure is probably due to the larger intermolecular separations in the solid state, which reduce dipolar broadenings. The previously determined parameters proved to be a suitable starting point for the fits to this spectrum. However, the predictably poorer

resolution of the hyperfine interactions, as well as some additional features in the lateral (intermultiplet) absorptions, add some uncertainty to these fits. Accordingly, these are treated as simulations and the results are given without a detailed statistical treatment. These are:  $g_{i||} = 2.230$ ,  $g_{i\perp} = 2.061$ ,  $\sigma_G = 3.31$  mT<sub>pp</sub>,  $\sigma_L = 3.85$  mT<sub>pp</sub>,  $r_{ij} = 8.22$  Å,  $J_{av} = 0.078$  cm<sup>-1</sup>,  $\Delta J = 0.011$  cm<sup>-1</sup>,  $A_{i||} = 540.0$  MHz,  $A_{i\perp} = 48.0$  MHz.  $\Delta_A$  was fixed to [0, 0, 0].

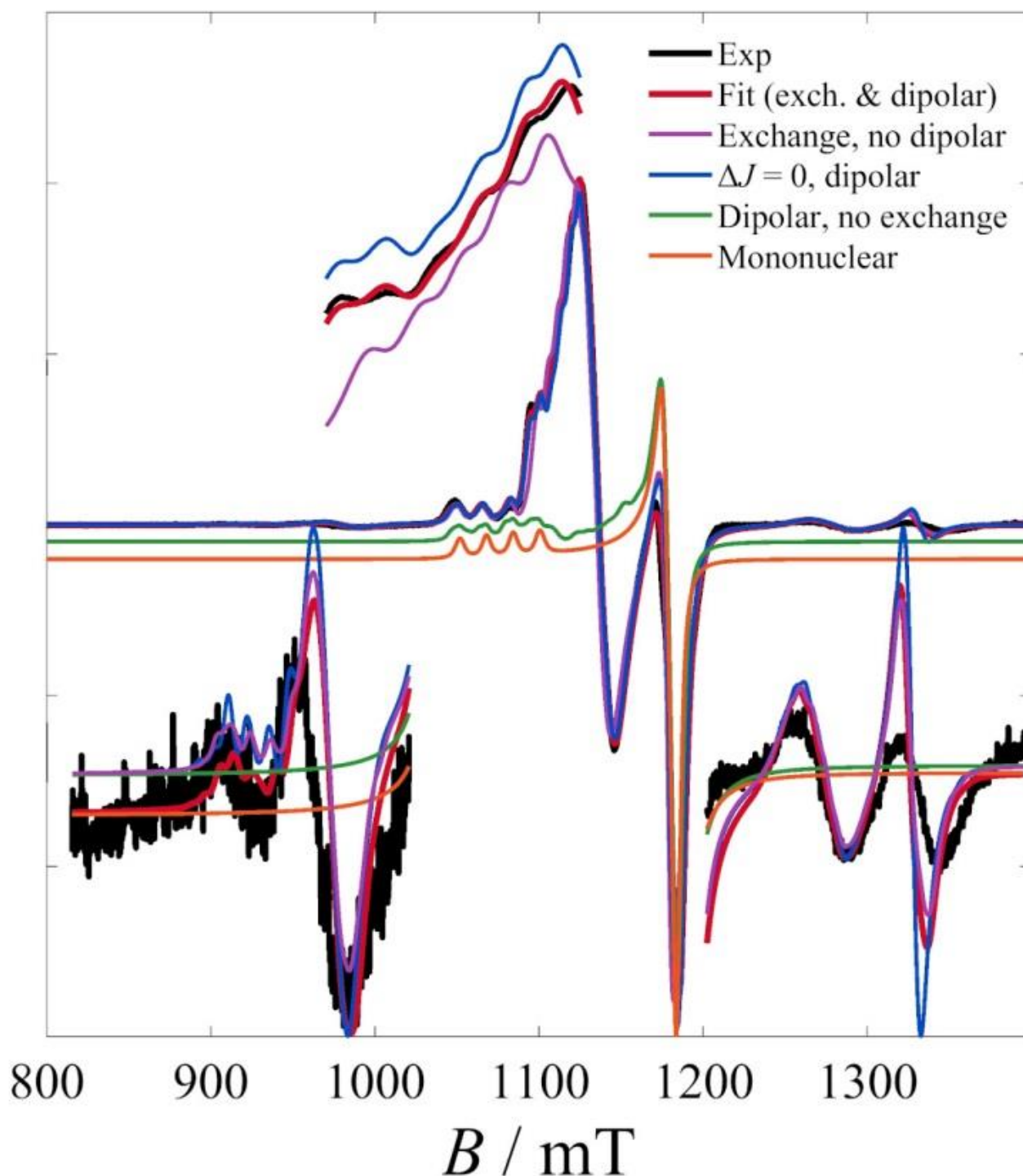


**Figure 6.** Effect of exchange terms to the calculated spectrum of **1**. Neglecting any of the electron–electron interaction terms leads to the spectra of visibly worse agreement to the experimental one.

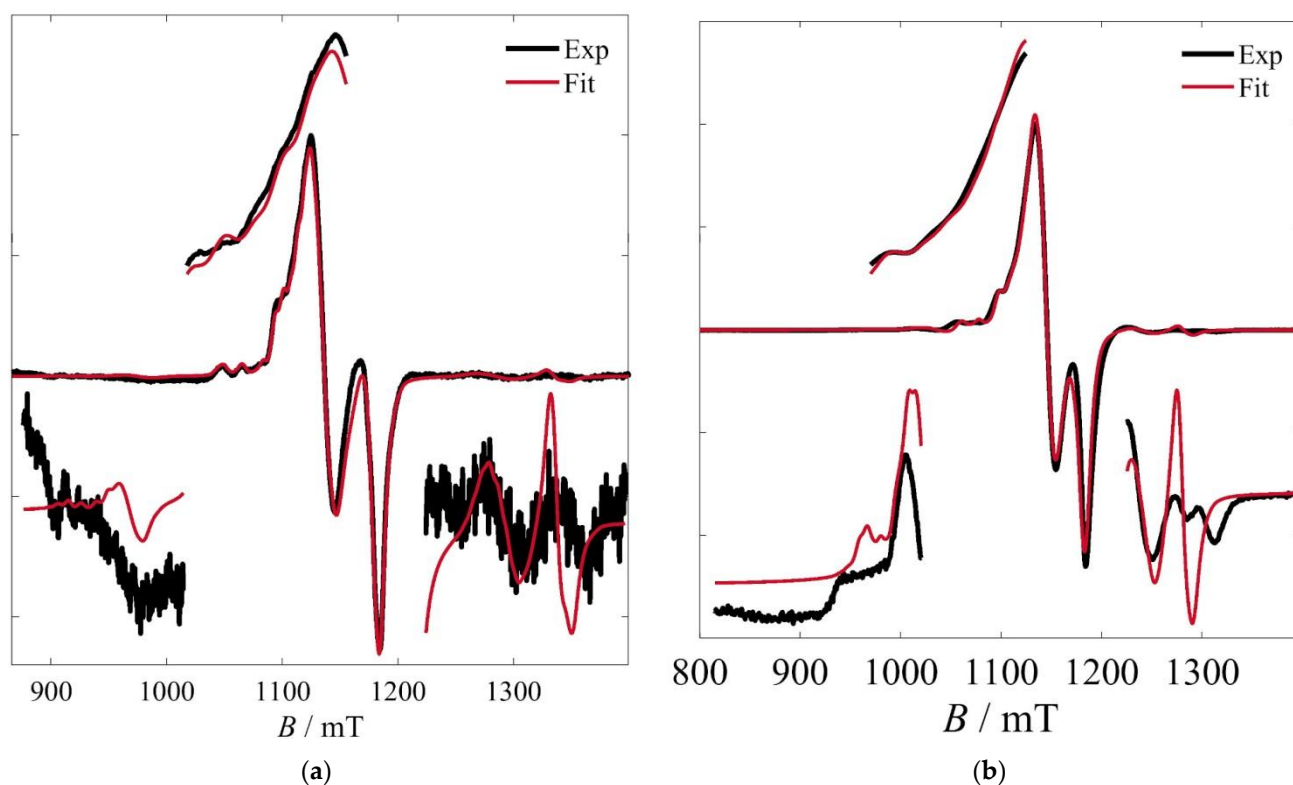


**Figure 7.** (a) Q-band spectrum from a frozen solution of **2** at 5 K and best fits according to the model and parameters described in the text. (b) Q-band spectrum from a powdered sample of **3** at 295 K and simulation according to the model and parameters described in the text.

### 3. Discussion and Comparative Analyses

This work demonstrates that EPR spectroscopy can be successfully used to address weak spin–spin interactions in relatively complicated polynuclear systems, thus providing an important complement to magnetometric studies. Indeed, the detailed EPR study of **1–3** allowed the estimation of very weak exchange interactions as well as dipolar couplings to a level of confidence practically unattainable with magnetic susceptometry experiments. Notably, a single EPR experiment for each complex provided sufficient information for the determination of those interactions in parallel to hyperfine ones.

As far as the specific complexes of this study are concerned, these were shown to exhibit a close agreement in their magnetic properties (Table 1), in accordance to their very similar molecular structures. Regarding the exchange and hyperfine interactions, the rationalization of their precise magnitudes requires the use of theoretical models, which is beyond the scope of this work. However, regarding the larger line widths of **3**, these may plausibly be attributed to remaining intermolecular dipolar interactions in the solid state, which give rise to smaller but non-negligible dipolar broadenings.

It should be noted that similar systems have been studied in the past, using EPR spectroscopy at even higher fields like in the case of  $\text{Cu}^{\text{II}}_3$  triangles encapsulated in polyoxometallates. In particular, the powder W-band EPR spectra of  $\text{K}_9\text{Na}[\text{Cu}_3(\text{H}_2\text{O})_3(\alpha\text{-TeW}_9\text{O}_{33})_2] \cdot 16\text{H}_2\text{O}$  [17] and  $\text{Na}_9[\text{Cu}_3\text{Na}_3(\text{H}_2\text{O})_9(\alpha\text{-AsW}_9\text{O}_{33})_2] \cdot 26\text{H}_2\text{O}$  [18] were simulated by a giant spin approach, with the exchange interactions determined independently by variable-temperature magnetic susceptometry. Subsequently, single-crystal studies of the latter complex were complemented by pulsed field-sweep experiments for the same purpose [19,20]. Despite the clear presence of intermultiplet resonances in these latter spectra, these resonances were not simulated for the determination of exchange interactions.

**Table 1.** Spin–Hamiltonian parameters of 1–3 as determined from fits to frozen solution (1, 2) and powder (3) Q-band EPR spectra.

	1	2	3
$g_{i  }$	$2.25707 \pm 0.00036$	$2.25488 \pm 0.00061$	2.230
$g_{i\perp}$	$2.05853 \pm 0.00021$	$2.06111 \pm 0.00025$	2.061
$\sigma_G/\sigma_L$ (mT <sub>pp</sub> )	$2.31 \pm 0.80/2.85 \pm 0.22$	$3.3 \pm 1.0/2.41 \pm 0.50$	3.3/3.9
$r_{ij}$ (Å)	$8.22 \pm 0.11$	$8.35 \pm 0.15$	8.22
$J_{av}$ (cm <sup>-1</sup> )	$0.11217 \pm 0.00050$	$0.11628 \pm 0.00073$	0.078
$\Delta J$ (cm <sup>-1</sup> )	$0.0114 \pm 0.0018$	$0.0150 \pm 0.0019$	0.011
$A_{i  }$ (MHz)	$502.94 \pm 8.42$	$543 \pm 14$	540
$A_{i\perp}$ (MHz)	$52.0 \pm 13.$	$69.6 \pm 6.4$	48
$\Delta_A$ (°)	$[-6.4 \pm 2.5, 3.4 \pm 7.4, 28.8486 \pm 0.0005]$	[0, 0, 0]	[0, 0, 0]

Of relevance are also studies of the extensively explored polyoxovanadate system  $K_6[V_{15}As_6O_{42}(H_2O)] \cdot 8H_2O$ , or “V<sub>15</sub>”, whose precise determination of the spin–spin interactions has been a contentious issue. The metallic core of the molecule can be considered as three-layered, i.e., {V<sub>6</sub>-V<sub>3</sub>-V<sub>6</sub>}, with the top and bottom “V<sub>6</sub>” layers exhibiting strong anti-ferromagnetic interactions, which quench their magnetizations. Thus, the low-temperature magnetic properties of the molecule are usually treated as stemming from the weakly coupled triangular “V<sub>3</sub>” layer [21]. It is of note that while extensive studies have been conducted, employing an arsenal of techniques, such as various types of magnetometry [22,23], EPR at various frequencies [24], inelastic neutron scattering [25], heat capacity [26] and NMR spectroscopy [27], there still remain ambiguities around the precise nature of the spin–spin interactions of this molecule. The application of the models described in this work should complement our understanding of this question.

#### 4. Conclusions

Overall, the development of detailed models integrating exchange and dipolar interactions can be very useful for the determination of very weak such interactions and allow for the full unlocking of the information contained in EPR spectra. Indeed, the broad availability of EPR simulation tools, such as *Easyspin* [28] or *Phi* [29], that consider arbitrary multispin Hamiltonians, makes the development of such models a tractable task, albeit not a routine one. Moreover, the increases in performance of computer processors over the past years have brought the unavoidable computational overhead of such models within the reach of even personal computers.

The combination of the above can allow for the detailed description of the magnetic spectra of a large number of weakly interacting molecular or biological polynuclear systems, currently beyond the reach of magnetometric techniques. On the one hand, the new information gleaned from the detailed treatment of EPR spectra should be particularly useful in refining first-principles theoretical models that attempt to determine such interactions from known molecular structures; the accurate determinations of weak exchange would push these models to their limits and reveal avenues for their improvement. On the other hand, this information would be helpful in the structural elucidation of biological systems from their EPR signatures; the structures of metalloenzyme active sites containing poly-metallic weakly coupled magnetic cores could be deduced in the absence of high-resolution crystal data.

In conclusion, the implementation of such detailed models should complement the understanding of multispin molecular or biological systems, even using powder/frozen solution EPR spectra.

## 5. Experimental Section

### 5.1. Syntheses

*Dipyatriz.* The synthesis was carried out according to the process described in the literature [30]. Recrystallization of 4.4 g of the crude product was carried out by dissolving in 120 mL of warm  $\text{CH}_2\text{Cl}_2$  and precipitating by the addition of *n*-hexane. After filtration and drying, the yield was 2.2 g of pure ligand.

*Complex 1.* This was synthesized according to the process described in the literature using a stoichiometric reaction of the starting materials [13]. The blue powder that precipitated was analyzed as  $1 \cdot 4.6\text{H}_2\text{O}$  (0.903 g, 52% on ligand basis or metal basis) and slow evaporation of the filtrate yielded single crystals whose unit cell determination matched the published structure.

*Complex 2.* This was first reported in [13] as an accidental product and its synthesis has now been rationalized. In particular, solid dipyatriz (0.214 g, 0.360 mmol) was added to a MeOH solution (110 mL) containing  $\text{CuCl}_2 \cdot 2\text{H}_2\text{O}$  (0.0460 g, 0.270 mmol) and  $\text{Cu}(\text{ClO}_4)_2 \cdot 6\text{H}_2\text{O}$  (0.100 g, 0.270 mmol). In the absence of full dissolution of the ligand, 35 mL of MeCN was added to the mixture, causing full dissolution in a few minutes and a deep blue solution. In three days, good parallelepiped crystals had formed, whose unit cell determination confirmed their identity. The yield was 37.3 mg (9%).

*Complex 3.* This was synthesized according to the procedure reported in [14].

### 5.2. EPR Spectroscopy

CW EPR spectra were collected on an EMXplus spectrometer (Bruker BioSpin GmbH, Germany) controlled using the Bruker Xenon software (Version 1.1b.44, Bruker BioSpin GmbH, Germany), with the magnetic field applied via a Bruker BE25 electromagnet using a Bruker ER082(155/45)Z (Bruker BioSpin GmbH, Germany) power supply.

For X-band experiments, the spectrometer was fitted with an EMX microX bridge (Bruker BioSpin GmbH, Germany) and a Bruker ER4122SHQE (Bruker BioSpin GmbH, Germany) cavity operating in the  $\text{TE}_{011}$  mode. Low-temperature experiments were carried out using an ESR900 (Oxford Instruments, UK) dynamic continuous flow cryostat and the temperature was regulated with an Oxford ITC4 (Oxford Instruments, UK) servocontrol. For Q-band spectra, the spectrometer was fitted with an EMX premiumQ microwave bridge and an ER5106QTW microwave resonator (Bruker BioSpin GmbH, Germany) operating in the  $\text{TE}_{012}$  mode. For low-temperature experiments, the resonator was fitted in an Oxford CF935 (Oxford Instruments, UK) dynamic continuous flow cryostat and the temperature was regulated with an Oxford ITC503 (Oxford Instruments, UK) servocontrol.

Fits to the EPR data and simulations were carried out with *Easyspin* v. 6.0 using custom-made routines [28].

The EPR solutions of **1** (0.54 mM in MeOH for the X-band experiments and 1.34 mM in MeOH/MeCN 50:50 for the Q-band experiments), **2** (0.84 mM in MeCN) and **3** (0.40 mM in MeCN) were deoxygenated with freeze–pump–thaw cycles, flame-sealed under a helium atmosphere in the EPR tubes and stored in liquid nitrogen.

**Supplementary Materials:** The following supporting information can be downloaded at: <https://www.mdpi.com/article/10.3390/magnetochemistry9100217/s1>, Figure S1: Fits for complex **1** considering different isotopologues; Figure S2: Low-field Zeeman diagram for complex **1**.

**Funding:** This project has received funding from the European Union's Horizon 2020 research and innovation program under the Marie Skłodowska-Curie grant agreement No. 746060 (project "CHIRALQUBIT").

**Institutional Review Board Statement:** Not applicable.

**Informed Consent Statement:** Not applicable.

**Data Availability Statement:** The data that support the findings of this study are available from the author upon reasonable request.

**Acknowledgments:** I particularly wish to thank Romain Ruppert for the synthesis of the ligand.

**Conflicts of Interest:** The author declares no conflict of interest.

## References

1. Boudalis, A. Half-Integer Spin Triangles: Old Dogs, New Tricks. *Chem. A Eur. J.* **2020**, *27*, 7022–7042. [[CrossRef](#)] [[PubMed](#)]
2. Boudalis, A.K.; Robert, J.; Turek, P. First Demonstration of Magnetoelectric Coupling in a Polynuclear Molecular Nanomagnet: Single-Crystal EPR Studies of  $[\text{Fe}_3\text{O}(\text{O}_2\text{CPh})_6(\text{Py})_3]\text{ClO}_4 \cdot \text{py}$  under Static Electric Fields. *Chem. Eur. J.* **2018**, *24*, 14896–14900. [[CrossRef](#)] [[PubMed](#)]
3. Robert, J.; Parizel, N.; Turek, P.; Boudalis, A.K. Polyanisotropic Magnetoelectric Coupling in an Electrically Controlled Molecular Spin Qubit. *J. Am. Chem. Soc.* **2019**, *141*, 19765–19775. [[CrossRef](#)] [[PubMed](#)]
4. Liu, J.; Mrozek, J.; Myers, W.K.; Timco, G.A.; Winpenny, R.E.P.; Kintzel, B.; Plass, W.; Ardavan, A. Electric Field Control of Spins in Molecular Magnets. *Phys. Rev. Lett.* **2019**, *122*, 037202. [[CrossRef](#)]
5. Kintzel, B.; Fittipaldi, M.; Böhme, M.; Cini, A.; Tesi, L.; Buchholz, A.; Sessoli, R.; Plass, W. Spin-Electric Coupling in a Cobalt(II)-Based Spin Triangle Revealed by Electric-Field-Modulated Electron Spin Resonance Spectroscopy. *Angew. Chem. Int. Ed.* **2021**, *60*, 8832–8838. [[CrossRef](#)]
6. Lewkowitz, M.; Adams, J.; Sullivan, N.S.; Wang, P.; Shatruk, M.; Zapf, V.; Arvij, A.S. Direct Observation of Electric Field-Induced Magnetism in a Molecular Magnet. *Sci. Rep.* **2023**, *13*, 2769. [[CrossRef](#)]
7. Trif, M.; Troiani, F.; Stepanenko, D.; Loss, D. Spin-Electric Coupling in Molecular Magnets. *Phys. Rev. Lett.* **2008**, *101*, 217201. [[CrossRef](#)]
8. Trif, M.; Troiani, F.; Stepanenko, D.; Loss, D. Spin Electric Effects in Molecular Antiferromagnets. *Phys. Rev. B* **2010**, *82*, 045429. [[CrossRef](#)]
9. Troiani, F.; Stepanenko, D.; Loss, D. Hyperfine-Induced Decoherence in Triangular Spin-Cluster Qubits. *Phys. Rev. B* **2012**, *86*, 161409. [[CrossRef](#)]
10. Stepanenko, D.; Trif, M.; Tsypliyatyev, O.; Loss, D. Field-Dependent Superradiant Quantum Phase Transition of Molecular Magnets in Microwave Cavities. *Semicond. Sci. Technol.* **2016**, *31*, 094003. [[CrossRef](#)]
11. Bencini, A.; Gatteschi, D.; Bencini, A. *EPR of Exchange Coupled Systems*; Dover Publications, Inc.: Mineola, NY, USA, 2012; ISBN 978-0-486-48854-7.
12. Mathivathanan, L.; Rogez, G.; Ben Amor, N.; Robert, V.; Raptis, R.G.; Boudalis, A.K. Origin of Ferromagnetism and Magnetic Anisotropy in a Family of Copper(II) Triangles. *Chem. Eur. J.* **2020**, *26*, 12769–12784. [[CrossRef](#)] [[PubMed](#)]
13. Barrios, L.A.; Aromí, G.; Frontera, A.; Quiñonero, D.; Deyà, P.M.; Gamez, P.; Roubeau, O.; Shotton, E.J.; Teat, S.J. Coordination Complexes Exhibiting Anion $\cdots\pi$  Interactions: Synthesis, Structure, and Theoretical Studies. *Inorg. Chem.* **2008**, *47*, 5873–5881. [[CrossRef](#)] [[PubMed](#)]
14. Yuste, C.; Cañadillas-Delgado, L.; Labrador, A.; Delgado, F.S.; Ruiz-Pérez, C.; Lloret, F.; Julve, M. Low-Dimensional Copper(II) Complexes with the Trinucleating Ligand 2,4,6-Tris(Di-2-Pyridylamine)-1,3,5-Triazine: Synthesis, Crystal Structures, and Magnetic Properties. *Inorg. Chem.* **2009**, *48*, 6630–6640. [[CrossRef](#)]
15. Demeshko, S.; Leibel, G.; Dechert, S.; Meyer, F. 1,3,5-Triazine-Based Tricopper(Ii) Complexes: Structure and Magnetic Properties of Threefold-Symmetric Building Blocks. *Dalton Trans.* **2004**, 3782. [[CrossRef](#)]
16. Chen, J.; Wang, X.; Shao, Y.; Zhu, J.; Zhu, Y.; Li, Y.; Xu, Q.; Guo, Z. A Trinuclear Copper(II) Complex of 2,4,6-Tris(Di-2-Pyridylamine)-1,3,5-Triazine Shows Prominent DNA Cleavage Activity. *Inorg. Chem.* **2007**, *46*, 3306–3312. [[CrossRef](#)] [[PubMed](#)]
17. Stowe, A.C.; Nellutla, S.; Dalal, N.S.; Kortz, U. Magnetic Properties of Lone-Pair-Containing, Sandwich-Type Polyoxoanions: A Detailed Study of the Heteroatomic Effect. *Eur. J. Inorg. Chem.* **2004**, 2004, 3792–3797. [[CrossRef](#)]
18. Kortz, U.; Nellutla, S.; Stowe, A.C.; Dalal, N.S.; van Tol, J.; Bassil, B.S. Structure and Magnetism of the Tetra-Copper(II)-Substituted Heteropolyanion  $[\text{Cu}_4\text{K}_2(\text{H}_2\text{O})_8(\alpha\text{-AsW}_9\text{O}_{33})_2]^{8-}$ . *Inorg. Chem.* **2004**, *43*, 144–154. [[CrossRef](#)]
19. Choi, K.-Y.; Matsuda, Y.H.; Nojiri, H.; Kortz, U.; Hussain, F.; Stowe, A.C.; Ramsey, C.; Dalal, N.S. Observation of a Half Step Magnetization in the  $\{\text{Cu}_3\}$ -type Triangular Spin Ring. *Phys. Rev. Lett.* **2006**, *96*, 107202. [[CrossRef](#)]
20. Choi, K.-Y.; Dalal, N.S.; Reyes, A.P.; Kuhns, P.L.; Matsuda, Y.H.; Nojiri, H.; Mal, S.S.; Kortz, U. Pulsed-Field Magnetization, Electron Spin Resonance, and Nuclear Spin-Lattice Relaxation in the  $\{\text{Cu}_3\}$  Spin Triangle. *Phys. Rev. B* **2008**, *77*, 024406. [[CrossRef](#)]
21. Gatteschi, D.; Pardi, L.; Barra, A.L.; Müller, A.; Döring, J. Layered Magnetic Structure of a Metal Cluster Ion. *Nature* **1991**, *354*, 463–465. [[CrossRef](#)]
22. Tarantul, A.; Tsukerblat, B.; Müller, A. High-Field Magnetization of V<sub>15</sub> Cluster at Ultra-Low Temperatures: Importance of Antisymmetric Exchange and Its Precise Estimation. *Chem. Phys. Lett.* **2006**, *428*, 361–366. [[CrossRef](#)]
23. Tarantul, A.; Tsukerblat, B.; Müller, A. Static Magnetization of V<sub>15</sub> Cluster at Ultra-Low Temperatures: Precise Estimation of Antisymmetric Exchange. *Inorg. Chem.* **2007**, *46*, 161–169. [[CrossRef](#)] [[PubMed](#)]
24. Vongtragool, S.; Gorshunov, B.; Mukhin, A.A.; van Slageren, J.; Dressel, M.; Müller, A. High-Frequency Magnetic Spectroscopy on the Molecular Magnetic Cluster V<sub>15</sub>. *Phys. Chem. Chem. Phys.* **2003**, *5*, 2778–2782. [[CrossRef](#)]
25. Chaboussant, G.; Ochsenbein, S.T.; Sieber, A.; Güdel, H.-U.; Mutka, H.; Müller, A.; Barbara, B. Mechanism of Ground-State Selection in the Frustrated Molecular Spin Cluster V<sub>15</sub>. *EPL* **2004**, *66*, 423–429. [[CrossRef](#)]
26. Fu, Z.; Xiao, Y.; Su, Y.; Zheng, Y.; Kögerler, P.; Brückel, T. Low-Lying Magnetic Excitations and Magnetocaloric Effect of Molecular Magnet  $\text{K}_6[\text{V}_{15}\text{As}_6\text{O}_{42}(\text{H}_2\text{O})] \cdot 8\text{H}_2\text{O}$ . *EPL* **2015**, *112*, 27003. [[CrossRef](#)]

27. Furukawa, Y.; Nishisaka, Y.; Kumagai, K.; Kögerler, P.; Borsa, F. Local Spin Moment Configuration in the Frustrated  $s = 1/2$  Heisenberg Triangular Antiferromagnet  $V_{15}$  Determined by NMR. *Phys. Rev. B* **2007**, *75*, 220402. [[CrossRef](#)]
28. Stoll, S.; Schweiger, A. EasySpin, a Comprehensive Software Package for Spectral Simulation and Analysis in EPR. *J. Magn. Reson.* **2006**, *178*, 42–55. [[CrossRef](#)]
29. Chilton, N.F.; Anderson, R.P.; Turner, L.D.; Soncini, A.; Murray, K.S. PHI: A Powerful New Program for the Analysis of Anisotropic Monomeric and Exchange-Coupled Polynuclear  $d$ - and  $f$ -Block Complexes. *J. Comput. Chem.* **2013**, *34*, 1164–1175. [[CrossRef](#)]
30. Pang, J.; Tao, Y.; Freiberg, S.; Yang, X.-P.; D'Iorio, M.; Wang, S. Syntheses, Structures, and Electroluminescence of New Blue Luminescent Star-Shaped Compounds Based on 1,3,5-Triazine and 1,3,5-Trisubstituted Benzene. *J. Mater. Chem.* **2002**, *12*, 206–212. [[CrossRef](#)]

**Disclaimer/Publisher's Note:** The statements, opinions and data contained in all publications are solely those of the individual author(s) and contributor(s) and not of MDPI and/or the editor(s). MDPI and/or the editor(s) disclaim responsibility for any injury to people or property resulting from any ideas, methods, instructions or products referred to in the content.